UNIVERSITY OF CALIFORNIA,
IRVINE

Piercing Mechanics of Bed Bug Tarsi

THESIS

submitted in partial satisfaction of the requirements
for the degree of

MASTER OF SCIENCES

in Biological Sciences

by

Jorge Bustamante, Jr.

Thesis Committee:
Senior Lecturer SOE Catherine Loudon, Chair
Professor Timothy J. Bradley
Associate Professor Matthew J. McHenry

2015

DEDICATION

To

my parents, friends, and former students

in recognition of their support, their kinship,

and the joy that they have brought to my life.

TABLE OF CONTENTS

LIST OF FIGURES

LIST OF TABLES

ACKNOWLEDGMENTS

I would like to express my deepest appreciation and gratitude to my committee chair, Dr. Catherine Loudon. Without the guidance, advice, effort, and attention to detail provided by Dr. Loudon this thesis would not be possible to complete. Transitioning from mechanical engineering to the realm of biology was heavily influenced by Dr. Loudon as an excellent mentor and advisor and partially my own sheer interest in the subject.

I would like to thank my committee members, Dr. Timothy J. Bradley and Dr. Matthew J. McHenry, whose continued guidance and advice aided in elevating the overall clarity, and structure of this thesis.

In addition, I would like to thank Dr. Timothy Rupert, and Jason Panzarino (Ph.D. student) for their continued collaboration on this project. The empirical measurements, and advice on analysis would not have been possible without their collaboration.

ABSTRACT OF THE THESIS

Piercing Mechanics of Bed Bug Tarsi

By

Jorge Bustamante, Jr.

Master of Sciences in Biological Sciences

University of California, Irvine, 2015

Dr. Catherine Loudon, Chair

The mechanical properties of bed bug (*Cimex lectularius* L.) tarsi were investigated in order to evaluate their vulnerability to piercing by plant trichomes (sharp microscopic hairs). This information will help inform development of physical methods for control of insect pests such as bed bugs. Nanoindentation was used to measure the force required to insert a sharp probe into the cuticle of the tarsi in different regions, as well as to determine creep and reduced elastic moduli for the cuticle. Scanning electron microscopy was used to visualize the indents that had been generated by nanoindentation. Scanning electron microscopy was also used to visualize the process of indent formation while poking the cuticle with a nanomanipulator. Focused ion beam milling was used to determine cuticle thickness for different regions of the tarsi. The force required to insert a sharp object into the cuticle of the tarsus was determined for depths ranging from 1 to 9 microns at strain rates ranging from 0.003 to 0.5 s^{-1}. Greater force was required to insert a sharp object at greater depth or at faster strain rates. A specific region of the pretarsal claws (membrane with microtrichia) was more frequently pierced by trichomes during bed bug locomotion, and was more easily pierced, exhibited more creep, and had a lower reduced elastic modulus. The combination of these mechanical attributes, in addition to the presence of natural

infoldings in the cuticle of this area, make the membrane with microtrichia of the pretarsal claws particularly vulnerable to piercing.

INTRODUCTION

The growing resurgence of bed bugs (*Cimex lectularius* L.), coupled with the evolution of resistance to chemical pesticides are stimulating the development of new non-chemical and non-toxic methods for bed bug control (Doggett et al., 2012; Hansen et al., 2011; Kells, 2006a; Kells, 2006b; Koganemaru and Miller, 2013). For hundreds of years in Europe, spreading leaves from bean plants around the sleeping quarters was a useful natural remedy to control bed bug populations (Potter, 2011; Richardson, 1943). Hook-like non-glandular trichomes grow on the undersurface of leaves from bean plants (*Phaseolus vulgaris*) with the function of protection against aphids and leafhoppers (Johnson, 1953). Coincidentally, the same trichomes that entrap aphids and leafhoppers also entrap bed bugs despite no direct co-evolutionary history between bed bugs and bean plants (Szyndler et al., 2013). The mechanism of entrapment by the hook-like plant trichomes was identified as piercing at specific locations of the tarsi: the undersurface of the pretarsal claws and in between the tarsal subsegments (Szyndler et al., 2013). Identifying the underlying physical cause for the mechanical vulnerability of these specific locations on the tarsi can aid in the development of non-toxic, non-chemical methods of bed bug entrapment.

Whether one object will pierce another will depend on the geometry of the objects, their material and structural properties, and relative motion. The specific mechanical barriers of the bed bug cuticle that must be overcome by the trichomes in order for piercing to occur remain unidentified. The method of nanoindentation can identify the relevant material properties at a sufficiently small microscopic scale for piercing of bed bug tarsi by plant trichomes. The original application for nanoindentation was to test homogenous, flat materials such as thin films and

crystalline structures. The application of nanoindentation has expanded to test various biological materials such as dentin (Kinney et al., 2003), bone (Huja et al., 2010), and even insect cuticle (Barbakadze et al., 2006; Broomell et al., 2008; Cribb et al., 2010; Kheireddin et al., 2012; Klocke and Schmitz, 2012; Kohane et al., 2003; Sample et al., 2015; Xiao et al., 2007), although none of the studies on insect cuticle used cuticle of legs or tarsi.

All studies of nanoindentation on insect cuticle except one (Kohane et al., 2003) used excised cuticle (cut from the insect). Excised cuticle dehydrates rapidly and changes in material properties over time, with the stiffness of the insect cuticle increasing as it dehydrates (Barbakadze et al., 2006; Broomell et al., 2008; Cribb et al., 2010; Kheireddin et al., 2012; Klocke and Schmitz, 2012; Kohane et al., 2003; Sample et al., 2015; Xiao et al., 2007). To counteract this problem, we implemented the novel method of performing nanoindentation on restrained, live, whole bed bugs at specific locations of their tarsi.

We entrapped more bugs on leaves and performed additional SEM to identify the piercing locations more precisely. We performed nanoindentation at specific locations on their tarsi in order to determine the forces required to move a sharp microscopic probe into the cuticle at these specific locations. From these forces measured using the nanoindenter it is possible to make some inferences about the material/structural mechanical properties of the cuticle at these locations. Because the cuticle cannot be visualized during nanoindentation, we examined the cuticle after nanoindentation in low vacuum SEM for any remaining plastic deformation. We also visualized the mechanical response to the cuticle during the process of indent formation using a nanomanipulator with low vacuum SEM (this latter technique allows control of probe

movement but has no associated force measurement capabilities). Additionally, we estimated the cuticle thickness at the different locations by focused ion beam milling and imaging the cut surfaces in SEM.

MATERIALS AND METHODS

Experimental insects

All bed bugs used in experiments were adult males (*Cimex lectularius*). Bugs were of the "Fort Dixon" strain and were supplied by the University of Kentucky. Bugs were not fed after eclosion to adults. Nanoindentation measurements were made on bugs 8-161 days after adult eclosion. Nanomanipulator measurements were made on bugs 51-56 days after adult eclosion.

Experimental plants

Kidney bean plants (*Phaseolus vulgaris*) were grown in the UCI greenhouse from seed (Johnny's Seeds, Winslow, ME, Product 2554). Individual leaves used for bed bug entrapment were trifoliate and node ≥ 1 because these are the leaves that are most effective in capturing bed bugs (Szyndler et al., 2013). All leaves used were < 90 mm in length (from tip of leaf to petiole attachment).

Scanning electron microscope (SEM) imaging

All low-vacuum scanning electron microscope (LV-SEM) imaging was performed on a FEI Quanta 3D FEG Dual Beam SEM (FEI, Hillsboro, Oregon) at 0.6 mbar and 5 kV. Bed bugs examined in LV-SEM were glued onto SEM stubs with an acrylic mounting system (VariDur high performance mounting system 20-3576, 20-3578, 2:1 mix of powder to liquid hardener by

volume; Buehler, Lake Bluff, IL) to restrict their movement, but they were still alive even after imaging and exposure to the vacuum.

High-vacuum scanning electron microscopy (HV-SEM) was performed on the same instrument at 1.94 X 10^{-5} mbar and 5 kV. Bed bugs examined in HV-SEM were either air-dried or critical point dried before sputter coating with iridium (5-7 nm, Ion Beam Sputtering/Etching System, South Bay Technology, San Clemente, CA).

LV-SEM images were used to determine the length and width of the tarsal subsegments for the six different legs (n = 120 legs on 23 different bugs; 1-6 legs were used per bug; 3 bugs had all six legs measured).

Determining specific locations of piercing

Bed bugs were placed on kidney bean leaves (*Phaseolus vulgaris*) and took a few steps before become entrapped by the hook-like trichomes on the leaves. Bed bugs were removed from leaves and placed dorsal surface down on carbon tape on SEM stubs. The bug tarsi were viewed in LV-SEM and examined for evidence of piercing. A total of ten bed bugs were used for these measurements.

Anatomy

In order to evaluate gross differences in morphology in the different legs, lengths and widths (diameters) of tarsal subsegments were measured from scanning electron micrographs using Canvas 15 (see Figure 1) for 23 bugs total. Out of the 23 bugs, 3 had measurements on all 6 legs, 1 had measurements on 4 legs, 2 had measurements on 3 legs, 8 had measurements on 2 legs, and 9 had measurements on 1 leg. Analyses were done on all 23 bugs and on just the 3 bugs with all 6 legs measured (to check for artefacts caused by unbalanced data).

Different regions on the tarsi were identified for comparison: the "membrane with microtrichia" (the established name for the region of the cuticle on the pretarsal claws covered with microscopic hairs or microtrichia (Snodgrass, 1935)), the "smooth claw" which will refer to the rest of the pretarsal claw, and the tarsal subsegments (tarsal subsegments 1-3, Figure 1).

Nanoindentation

Mechanical testing measurements were performed with a diamond cube-corner tip nanoindenter (Agilent G200 DCM II head, Santa Clara, CA). This probe type has a sharp tip that is pressed into the surface, making a characteristic 3-sided indent (Figure 2). For a cube corner ("trirectangular tetrahedron"), the relationship between the area of the triangular base (A_b) (the projected equilateral triangle viewed in Figure 2A) and the altitude of the tetrahedron (the depth of indentation, D) is

$$A_b = \frac{3\sqrt{3}}{2} D^2 = 2.598\, D^2 \quad (1)$$

and the relationship between the projected length of any of the 3 "legs" (α, seen in Figure 2B) and the depth of indentation is

$$\alpha = \sqrt{2}\, D \quad (2)$$

Four different strain rates were used: 0.003, 0.005, 0.02, and 0.5 s^{-1}. These are "true" strain rates (instantaneous rates of increase in length), not engineering strain rates (rates of increase in length compared to starting length). Strain rates ($\dot{\varepsilon}_i$) were evaluated directly from the raw displacement and time data by dividing the instantaneous rate of displacement by the average displacement during that same time period

$$\dot{\varepsilon}_i = \frac{(h_{i+1} - h_i)}{(t_{i+1} - t_i)} \Big/ \frac{(h_{i+1} + h_i)}{2} \quad (3)$$

or

$$\dot{\varepsilon}_i = 2\, \frac{(h_{i+1} - h_i)}{(h_{i+1} + h_i)(t_{i+1} - t_i)} \quad (4)$$

where h_i is the displacement corresponding to time t_i (a forward estimate). The instrument was used in strain rate controlled mode. Force and displacement were recorded continuously at 1.56

Hz for the two slowest strain rates, 3.12 Hz for the 0.02 s^{-1} strain rate and 200-250 Hz for the fastest strain rate. A stiffness detection criterion of 200 N/m was used.

Some indents were performed with cycling. During cycling, the probe was translated into the surface by micron increments, held at a constant force for a set period of time (60 seconds for a 0.005 s^{-1} strain rate and 5 seconds for a 0.5 s^{-1} strain rate), and then the probe was moved back until the force was lowered to 10% of its peak value, and then moved into the surface until the next micron increment (of total translation) was reached (Figures 3 and 4).

For nanoindentation, live bed bugs were mounted on SEM stubs with an acrylic mounting system as described above. Live bugs were mounted on their backs, with their dorsal surface in contact with the SEM stub so that the ventral side of the bug was accessible. The tarsi, abdomen, thorax, and head were all firmly fixed in place to minimize movement during experimentation. Bugs were still alive after nanoindentation. A total of 123 indents on 67 different legs of 47 different bugs were analyzed. Bugs were moved to the scanning electron microscope to visualize the indent using low vacuum SEM as described above (see Figure 2 for example).

Reduced elastic modulus was calculated from the nanoindenter output using established methods (Oliver and Pharr, 1992) with the recommended adjustments for viscoelastic materials such as polymers (Kinney et al., 2003; Ngan et al., 2005). The average displacement rate during creep, $\dot{h}_h$ is

$$\dot{h}_h = \frac{\text{total creep}}{\text{time of creep}} \tag{5}$$

where the "total creep" is Δx between points 1 and 2 in Figure 3B, and the time of creep is 5 seconds for the fast strain rate (0.5 s^{-1}) and 60 seconds for the slow strain rate (0.005 s^{-1}). The average unloading rate during the first 90% of unloading, $\dot{P}_u$, was calculated by

$$\dot{P}_u = \frac{0.9P_u}{t_{0.9,\ \text{unloading}}} \tag{6}$$

where P_u is the force at the beginning of unloading (the y value of point 2 on Figure 3B) and $t_{0.9,\ \text{unloading}}$ is the time difference from the beginning of unloading until the load has reached 10% of its initial unloading value (the time difference between points 2 and 3. This approach is slightly different from Kinney et al. (2003), who estimated $\dot{P}_u$ from the midpoint (in time) of the unloading curve. However, the rate of change of force during unloading is quite linear (Figure 4A), and therefore equation (6) should provide similar results to the approach in Kinney et al. (2003). The apparent stiffness, S, is output by the nanoindenter software, and is the slope of the linear fit to the initial 50% of the unloading part of the curve. The creep-corrected contact stiffness, S_e, is calculated as (Ngan et al., 2005)

$$\frac{1}{S_e} = \frac{1}{S} - \frac{\dot{h}_h}{\dot{P}_u} \tag{7}$$

The reduced elastic modulus, E_r, is calculated as

$$E_r = \frac{\sqrt{\pi} S_e}{2\sqrt{A_c}} \tag{8}$$

where A_c is the contact area calculated from the basic geometry of a tetrahedron (equation 1) substituting h_c in for the altitude, D:

$$A_c = \frac{3\sqrt{3}}{2} {h_c}^2 = 2.598 {h_c}^2 \tag{9}$$

where the contact depth, h_c, is calculated as

$$h_c = h_{\max} - \varepsilon \frac{P_{\max}}{S_e} \tag{10}$$

where $h_{\max}$ is the maximal displacement during the cycle (x value of point 2 in Figure 3B) and ε is a number dependent on probe tip geometry, which is 0.72 for both the cube corner and Berkovich tip shapes (Oliver and Pharr, 1992).

Calculation of the elastic modulus, E, from the reduced elastic modulus, E_r, requires knowing the Poisson's ratio, v, for the cuticle and the indenter (Oliver and Pharr, 1992)

$$\frac{1}{E_r} = \left(\frac{1 - v^2}{E}\right)_{\text{sample}} + \left(\frac{1 - v^2}{E}\right)_{\text{indenter}} \tag{11}$$

The indenter probe tip is made of diamond. The relevant properties for diamond are $\nu_{diamond}$ = 0.07 (dimensionless) and $E_{diamond}$ = 1143 GPa (Klein, 1992).

Creep

Creep was measured during nanoindentation as the continued displacement into the cuticle when force was held constant for a set period of time. Creep was measured during cycling. For the fast cycling, the force was held constant for five seconds after every additional micron of displacement. For the slow cycling, the force was held constant for 60 seconds after every additional micron of displacement.

Visualization of cuticle deformation with a nanomanipulator

A nanomanipulator (Omniprobe 200, Oxford Instruments, Oxford UK) was used while bugs were in LV-SEM (FEI Quanta 3D FEG Dual Beam SEM) to visualize the events that occur when deforming bed bug cuticle with a sharp probe (such as during nanoindentation, which can't be observed directly). To facilitate comparison with the nanoindenter data, the nanomanipulator deformations were also made on the third tarsal subsegment and the two regions of the pretarsal claws. The shape of the nanomanipulator probe tip was similar to the nanoindentation probe, with a sharp corner, and is solid tungsten.

The nanomanipulator probe was moved to a position where it lightly made contact with the surface of the bed bug cuticle without deforming the cuticle. The nanomanipulator probe was then moved into the cuticle at a strain rate of 0.5 s^{-1} for either a target depth in the range 1-8 microns. Displacement into the surface of the cuticle was verified by removing the probe in 1 micron increments until the nanomanipulator probe had clearly lost contact with the surface.

Images were taken before insertion of the nanomanipulator probe, during the maximum translation of the nanomanipulator probe, and after removal of the nanomanipulator probe in order to categorize the type of deformation (e.g. plastic vs. elastic) (Figure 5). A total of 5 legs from 5 bugs (1 leg from each bug) were each poked at least one time on each of the 3 regions per leg: smooth area on pretarsal claws, membrane with microtrichia on pretarsal claws, and tarsal subsegments. A total of 35 pokes ranging from 1-10 microns in depth were made.

Focused ion beam (FIB) milling to determine cuticle thickness

FIB was performed on the FEI Quanta 3D FEG Dual Beam SEM (FEI, Hillsboro, Oregon) at 1.94 X 10^{-5} mbar, 16-30 kV and 15 nA. FIB uses a beam of gallium ions for milling. Specimens were air-dried or critical point dried and sputter-coated with Iridium (5-7 nm deep) before milling with FIB. At least three tarsi on each of three bugs were milled in the claw and tarsal subsegments to allow estimation of cuticle thickness from SEM images (tiff) recorded while milling. The images (1024 X 943 pixels) were imported into Canvas 15 (ACDSee, Seattle, WA), the scale determined by the scale bar on the image, and the cuticle thickness measured from the image to the nearest micron.

Statistics

Statistical tests were performed using SAS 9.4 (SAS, Cary, NC). The Proc GLM (General Linear Models) procedure was used for two-way ANOVAs, the interaction terms were included, and Type III results are reported (in this model the order of the parameters does not matter, because each effect is adjusted for all other effects) (SAS Institute Inc., 2008).

RESULTS

Anatomy

As is true for many bugs (Order Hemiptera), there are three tarsal subsegments (= tarsomeres) and paired pretarsal claws on each of the six legs (Woodward et al., 1970). The three tarsal subsegments are significantly different from each other in both length and diameter (Figure 1, Table 1, tarsal subsegments are numbered from proximal to distal). Length and diameter of tarsal subsegments are also significantly different for the three different leg types (forelegs, midlegs, and hindlegs), but were not significantly different for the left leg vs. the corresponding right leg. Although orientation (ventral view vs side view) did have a significant effect on diameter, the magnitude was extremely small (average 4% difference in ventral vs. side view) and not consistent, sometimes being larger for the ventral view and sometimes for the side view; therefore we will combine the measurements taken from the different orientations. Orientation did not have a significant effect on length (ANOVA on length; $P < 0.0001$ for leg type and subsegment, $P > 0.1$ for left vs. right side and for orientation) (ANOVA on diameter; $P < 0.001$ for leg type, subsegment and orientation, $P > 0.2$ for left vs. right side). Comparable results were found when the analysis was run only for the three bugs on which all legs were measured, and therefore the larger (unbalanced) data set is provided.

Table 1 Average diameter and length of tarsal subsegments							
		Diameter			Length		
Tarsal subsegment	**leg**	**Mean µm**	**STD µm**	***N***	**Mean µm**	**STD µm**	***N***
1	F	39.5	1.9	7	85.0	22.7	6
	M	42.0	3.7	7	102.8	13.9	7
	H	40.4	2.9	10	115.4	13.2	9
2	F	41.9	3.9	16	98.9	6.6	14
	M	45.5	4.7	15	104.2	9.5	14
	H	47.4	5.5	13	117.4	7.0	12
3	F	46.1	3.0	21	135.4	13.5	19
	M	49.6	3.6	16	131.7	14.8	16
	H	51.2	2.8	15	151.4	3.9	14
F = foreleg, M = midleg, H = hindleg STD = standard deviation, *N* = sample size							

Location of piercing on bed bug tarsi

The specific locations of piercing were imaged and mapped as shown in Figure 6. After walking on the leaves from bean plants, each of ten bugs was pierced at least once (range 1-3 piercings/bug, average 2.0 piercings/bug). The tarsi were only pierced in two locations of cuticle: on the pretarsal claws (18/20 piercings, usually near the boundary of the membrane with microtrichia), and through the intersegmental membrane between tarsal subsegments (2/20 piercings) (Figure 6).

Focused ion beam (FIB) milling to determine cuticle thickness

The thickness of cuticle ranged between 2-6 microns for the tarsal subsegments (Figure 7). The complex shape of the pretarsal claws was reflected in the variability of the cuticle thickness. At the distal tips, the claws were completely solid, while closer to the proximal end, the claws had a complex arrangement of channels (Figure 7B right). Therefore the cuticle thickness was highly variable for the claws, ranging from 1-16 microns. Both the smooth cuticle and the membrane with microtrichia on the pretarsal claws showed such variation.

Nanoindentation

The force to indent one micron into the cuticle was significantly different for the different regions on the tarsus, and was significantly affected by the strain rate (Figure 8) (ANOVA on force at 1 micron for region and strain rate: $P = 0.0016$ and $df = 2$ for region; $P < 0.0001$ and $df = 3$ for strain rate; $n = 123$ indents total). The interaction term for region X strain rate was not significant ($P = 0.57$ when included in the ANOVA) and therefore was dropped as a term. The force to indent one micron into the cuticle was significantly lower for the membrane with microtrichia compared to the rest of the pretarsal claws or for the tarsal subsegments. The force to indent one micron into the cuticle was greater with faster strain rates (Figure 8).

It took a greater force to indent farther into the cuticle for all conditions and regions (Figure 9). The increase in force with displacement was appoximately linear (Figure 9), and therefore the slope of a line fitted to the first 5 microns of displacement for any indent (forced to

a zero intercept) could be used to characterize the increase in force as a single number for that indent. The force was affected by both region and the strain rate (Figure 9). For the slow strain rates (Figure 9A), region was significantly different (ANOVA on slopes for region: $P = 0.0005$ and $df = 2$, $n = 17$ indents). For the fast strain rates (Figure 9B and C), region was not significantly different, and there were no significant differences cycling vs. not cycling (ANOVA on slopes for region and cycling: $P = 0.16$ and $df = 2$ for region; $P = 0.6$ and $df = 1$ for cycling/not cycling, $n = 30$ indents). Comparing strain rates for the cycling indents (Figure 9A and B), the force was significantly higher with a faster strain rate for the membrane with microtrichia but not the tarsal subsegments, and was significantly different for the different regions for the slow strain rate but not the fast strain rate, leading to a significant interaction term (ANOVA on slopes for region and speed: $P = 0.0003$ and $df = 2$ for region; $P = 0.004$ and $df = 1$ for speed, and $P = 0.04$ and $df = 2$ for the interaction term region X speed).

Creep measurements

In all locations, the cuticle showed extensive creep (Figure 10), which was measured during nanoindentation while pausing and allowing creep after each micron of advancement into the surface. After each micron of advancement, the force was held at a constant value (for 5 seconds for the faster strain rate and 60 seconds for the slower strain rate), and the cuticle continued to creep (the nanoindentor tip continued to move into the cuticle). The magnitude of creep varied with both region and strain rate (Figure 10). After the first micron of indentation, creep was highest for the membrane with microtrichia and lowest for the tarsal subsegments, and higher with a faster strain rate (ANOVA of creep in first 5 seconds with two factors; $P = 0.0006$

for region and $P < 0.0001$ for strain rate; Type III Sum of Squares; interaction term was significant $P = 0.0068$). After 2, 3, 4, or 5 cycles of 1 micron increments of indentation, strain rate continued to be highly significant in affecting the amount of creep, but region was no longer consistently significant (ANOVA of creep in first 5 seconds with two factors: $P > 0.18$ for region and $P < 0.0001$ for strain rate; Type III Sum of Squares; interaction terms were not significant). When the ANOVA was run for one strain rate group at a time for the 2, 3, 4, or 5 cycles, region was significant for some depths (3, 4, and 5 microns) but only for the slower strain rate (0.005 s^{-1}) (one-way ANOVA of creep, $P < 0.05$ for region for 3, 4, or 5 microns and $P > 0.05$ for region at 2 microns).

Creep over the first five seconds was about 10 times as far for the faster strain rate, but the creep duration was 12 times longer for the slower strain rate (60 seconds vs. 5 seconds). When the total creep was compared for the two strain rates (creep in five seconds for the faster strain rate and in 60 seconds for the slower strain rate), the total creep was only about two times as far for the faster strain rate.

Elastic modulus measurements

Reduced elastic modulus was calculated from the nanoindentation data during unloading after each hold time for each micron cycle. Therefore, there are estimates of reduced elastic modulus at approximately one micron increments. These are not exactly one micron increments because of creep; reduced elastic modulus is reported based on the displacement after creep has occurred, and therefore if for a slightly larger displacement (Figure 11). For the slow strain rate,

reduced elastic modulus was significantly different for the regions for the first 5 microns only (Figure 11A) (separate one-way ANOVA for each displacement cycle, ; $P < 0.05$ for region for first 5 cycles, $P > 0.05$ for region for remaining 4 cycles; $df = 2$). For the fast strain rate, the reduced elastic modulus was significantly different for the regions for six out of the nine depths (Figure 11B) (separate one-way ANOVA for each displacement cycle, ; $P < 0.05$ for region for cycles 2-6 and 8, $P > 0.05$ for region for remaining cycles; $df = 2$). Reduced elastic modulus was not affected by strain rate for cuticle of the tarsal subsegments (Figure 11C) (separate one-way ANOVA for each displacement cycle, ; $P > 0.05$ for all cycles; $df = 2$). For the membrane with microtrichia on the pretarsal claws, reduced elastic modulus was affected by strain rate after the second micron (Figure 11D) (separate one-way ANOVA for each displacement cycle, ; $P > 0.05$ for strain rate for first 2 cycles, $P < 0.05$ for strain rate for remaining cycles; $df = 2$).

The elastic modulus can be calculated from the reduced elastic modulus (equation 11), if the Poisson's ratio for cuticle is known. Substituting in the values for diamond, it is clear that the term for the indenter (equation 11) is negligible, leaving the simplified relationship of

$$E = (1 - \upsilon_{\text{cuticle}}{}^2)E_r \qquad (12)$$

The Poisson's ratio for insect cuticle has been reported as varying between 0.02-0.1 (in the plane of the cuticle, locust intersegmental membrane cuticle on the ovipositor of adult female locusts, Vincent, 1990; different numbers graphed in Figure 4.12 of the same reference are assumed to be in error). If the Poisson's ratio for the bed bug cuticle is ≤ 0.1, this would mean that E would be within 1% of E_r (equation 12), and therefore is a close approximation. The reduced elastic

modulus is often reported because of the lack of information on the Poisson's ratio for insect cuticle (Muller et al., 2008)

Visualization of cuticle deformation with a nanomanipulator

Even a single micron movement of the sharp probe into the surface resulted in a visible plastic deformation of the cuticle in the smooth part of the claw or the tarsal subsegment (Figure 5). The part of the pretarsal claw that is not smooth (membrane with microtrichia) appears to rebound elastically up to 5 microns of movement, but is permanently damaged for > 5 microns of movement (Figure 5C).

DISCUSSION

We have identified the magnitude of the force required to indent the cuticle in various regions of the tarsus at various depths by a sharp object. The magnitude of the force to indent one micron into the cuticle was about 0.5 mN (averaging over all regions and strain rates). It takes a larger force to indent farther for all regions. The region of the pretarsal claws that is typically pierced, the membrane with microtrichia, differed in several respects from the other areas of cuticle on the tarsus: it was easier to pierce (about 20-30% less for a depth of 1 micron), it displayed more creep for the first 2 microns of depth, and it was less elastic than the smooth part of the claw or the tarsal subsegments. In addition, the membrane with microtrichia behaves differently from the other regions tested; when visualized in low vacuum SEM while poking with the sharp nanomanipulator, the membrane with microtrichia did not form the characteristic indentation shape as seen in the rest of the cuticle, but simply rebounded without visible damage to a depth of up to 5 microns when the nanomanipulator probe was retracted. All of these mechanical attributes, in addition to the presence of the natural infoldings in the cuticle of this area, make the membrane with microtrichia of the pretarsal claws particularly vulnerable to piercing.

It is unclear what role cuticle thickness has in determining the location or force needed to indent the cuticle on the tarsus. The cuticle thickness was highly variable for the pretarsal claws; when sections were examined after milling, it was clear that different regions could not be characterized as having a typical constant cuticle thickness. However, the piercing was usually at the boundary between the membrane with microtrichia and the smooth part of the claw,

suggesting that the infolding of the cuticle at that area helps to secure the tip of the trichome, analogous to a "starter hole" guiding a hammered nail. Cuticle thickness was less variable for the tarsal subsegments.

The time-dependent properties of cuticle suggest that more force would be required to pierce the tarsi if the tarsi were lifted more quickly during locomotion. However, tarsi that are lifted more quickly against a trichome will probably be generating a larger force against a stationary trichome, so walking more quickly would not generate protection. Insects (including bed bugs) tend to cycle their legs through tripodal movements at a high frequency (bed bugs cycle through all 6 legs at ~8 times/sec; Szyndler et al. 2013), which means that their tarsi are being impaled within a fraction of second. This is even faster than our fastest experimental strain rate, but we were constrained by machine capabilities. Evidentally bed bugs are generating sufficient force when lifting their feet from the surface to self-impale. This force has not yet been measured. We know of no documented cases in which insects move particularly slowly when around trichomes, although careful placement of tarsi to avoid trichomes has been documented in other insects (Voigt et al., 2007; Voigt and Gorb, 2010). In other piercing contexts, it suggests that piercing of cuticle by ovipositors by parastioid wasps or piercing of cuticle by the aedeagus during traumatic insemination in bed bugs could require less force if the piercing structure is moved more slowly.

Although force data were recorded to a probe movement of nine microns, whether or not a sharp object will penetrate and possibly ultimately pierce the cuticle will be largely determined by the mechanical interaction that occurs in the first few microns. No abrupt discontinuity was

seen in the force recordings even though the cuticle would eventually become punctured or permanently dented with sufficient depth, and we did puncture the tarsal subsegments with our experimental conditions. The deformations that we generated with our sharp probes were localized to the immediate area of the sharp probe. The nanoindenter and nanomanipulator probe tips that we used are cube corner with a sharp tip, and share that important similarity with real trichomes which have a sharp but conical tip.

The identification of the forces required to pierce bed bug cuticle and the mechanical properties of the cuticle should help to inform development of synthetic materials intended to functionally mimic the bed bug entrapping capabilities of leaves from bean plants. In addition, this mechanical characterization will help us understand the co-evolutionary arms race between trichome-armed plants and insects.

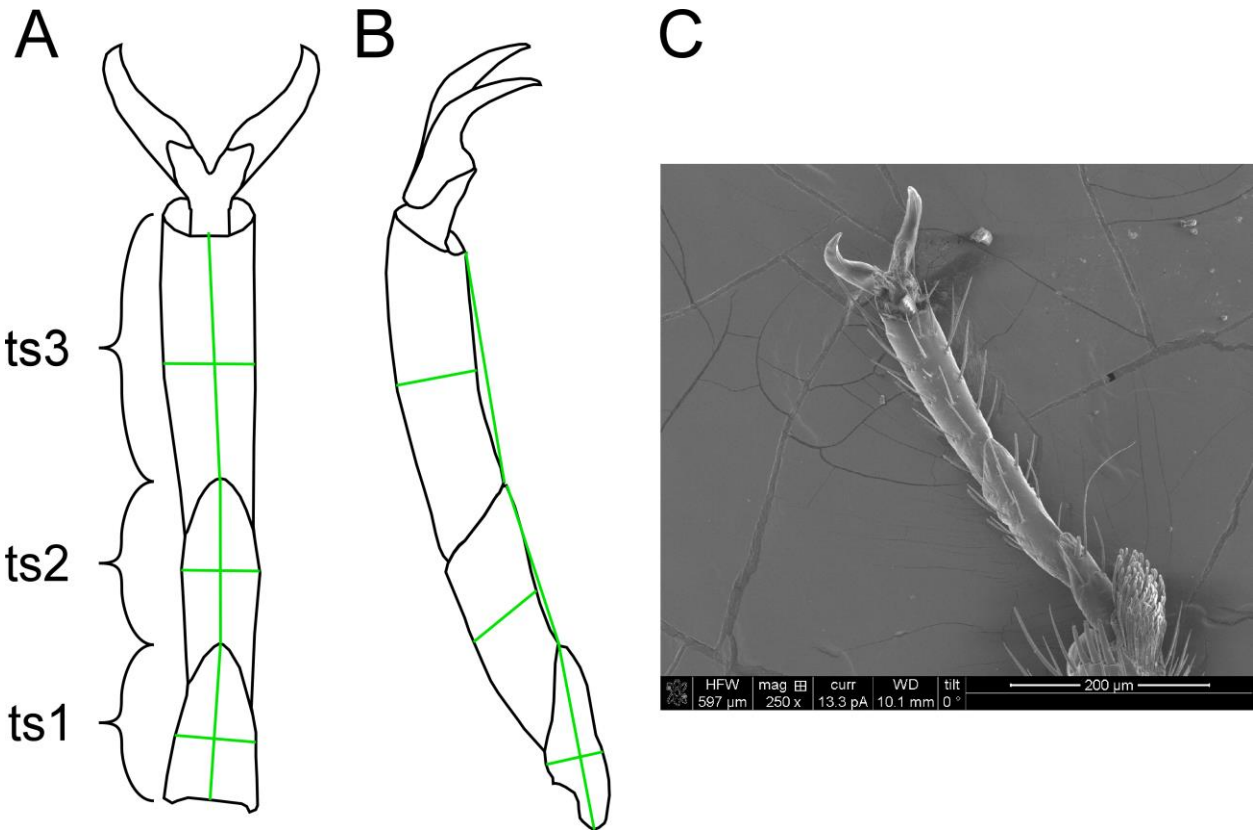

Figure 1. Measurement conventions for tarsal subsegments. The three tarsal subsegments (ts1, ts2, and ts3) are numbered from proximal to distal. Lengths (proximal-distal) and widths were measured as indicated by the green lines. All three of the legs have the same basic morphology. A. Ventral view of tarsus. B. Side view of tarsus. C. Scanning electron micrograph of ventral view of tarsus.

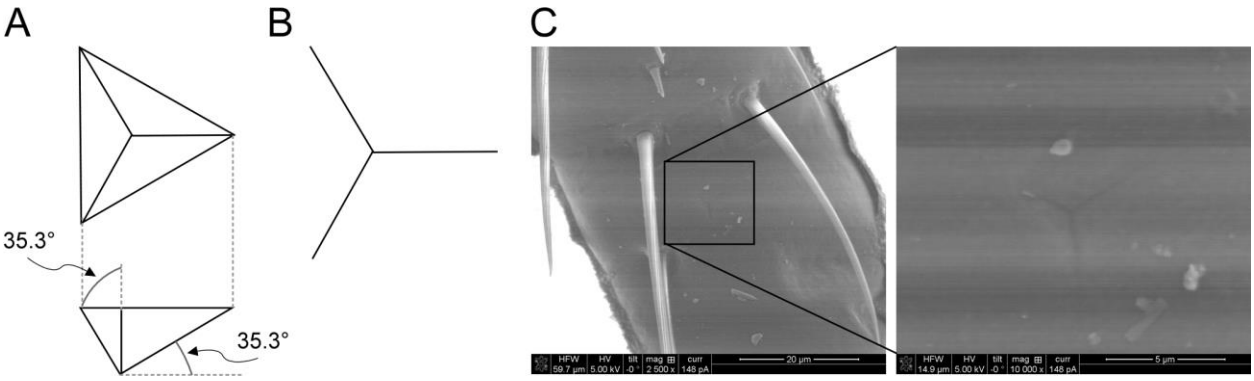

Figure 2. A. Geometry of nanoindenter tip of cube corner type. B. Shape of indent made by a cube corner tip. C. Scanning electron micrograph of tarsal subsegment 3 after nanoindentation. D. Higher magnification view of indent from (C).

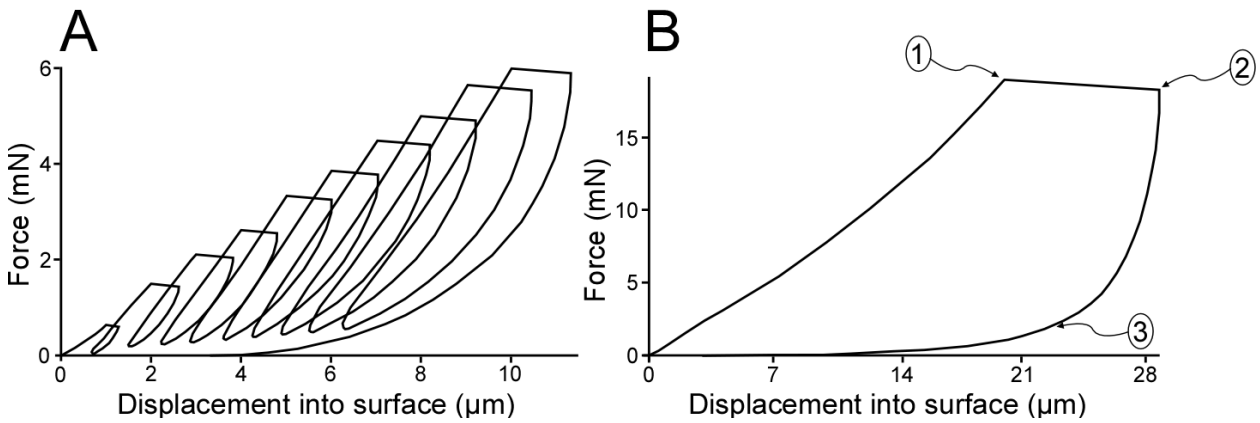

Figure 3. Example force and displacement output from the nanoindenter for cycling (A) and not cycling (B) indents. The "flat top" of the loops corresponds to the creep that occurs when the force is held constant (every micron of advancement for the cycling indent in A, and at the end of a single 20-micron advancement for the not-cycling indent in B). Points marked on B are used to describe how some of the calculations were made. Point 1 indicates the end of the loading portion of the cycle and the beginning of the hold time. Point 2 indicates the end of the hold time and the beginning of the unloading portion of the cycle. Point 3 indicates the point at which 10% of the peak load (measured at point 1) has been reached during unloading.

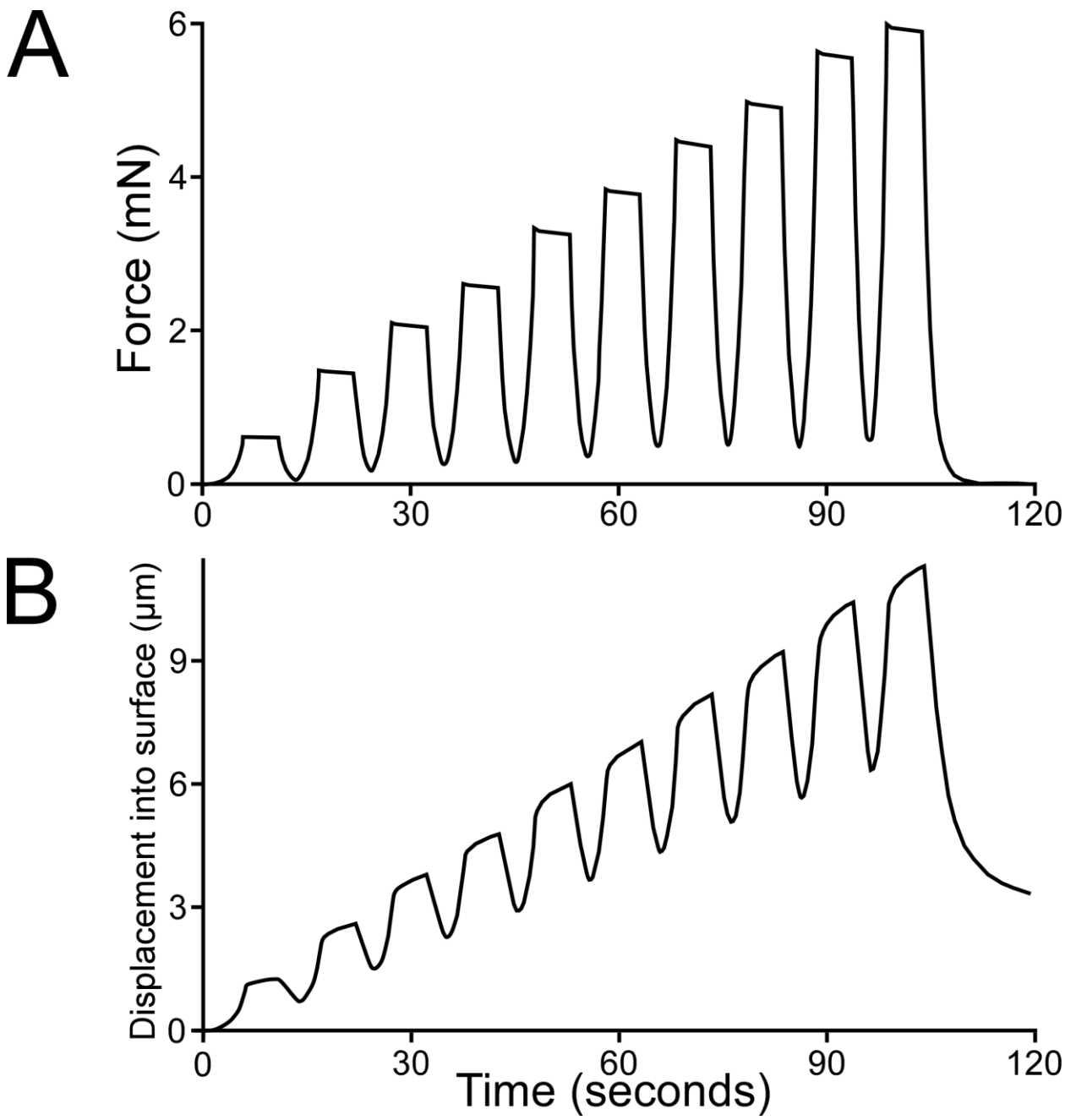

Figure 4. During a cycling indent, the force (A) and displacement (B) are both cycling with time as shown for the same example trace pictured in Figure 3(A). After each micron of advancement, the force is held constant (for 5 seconds in this trace), and then reduced to 10% of its peak value before increasing again until the next micron of advancement occurs.

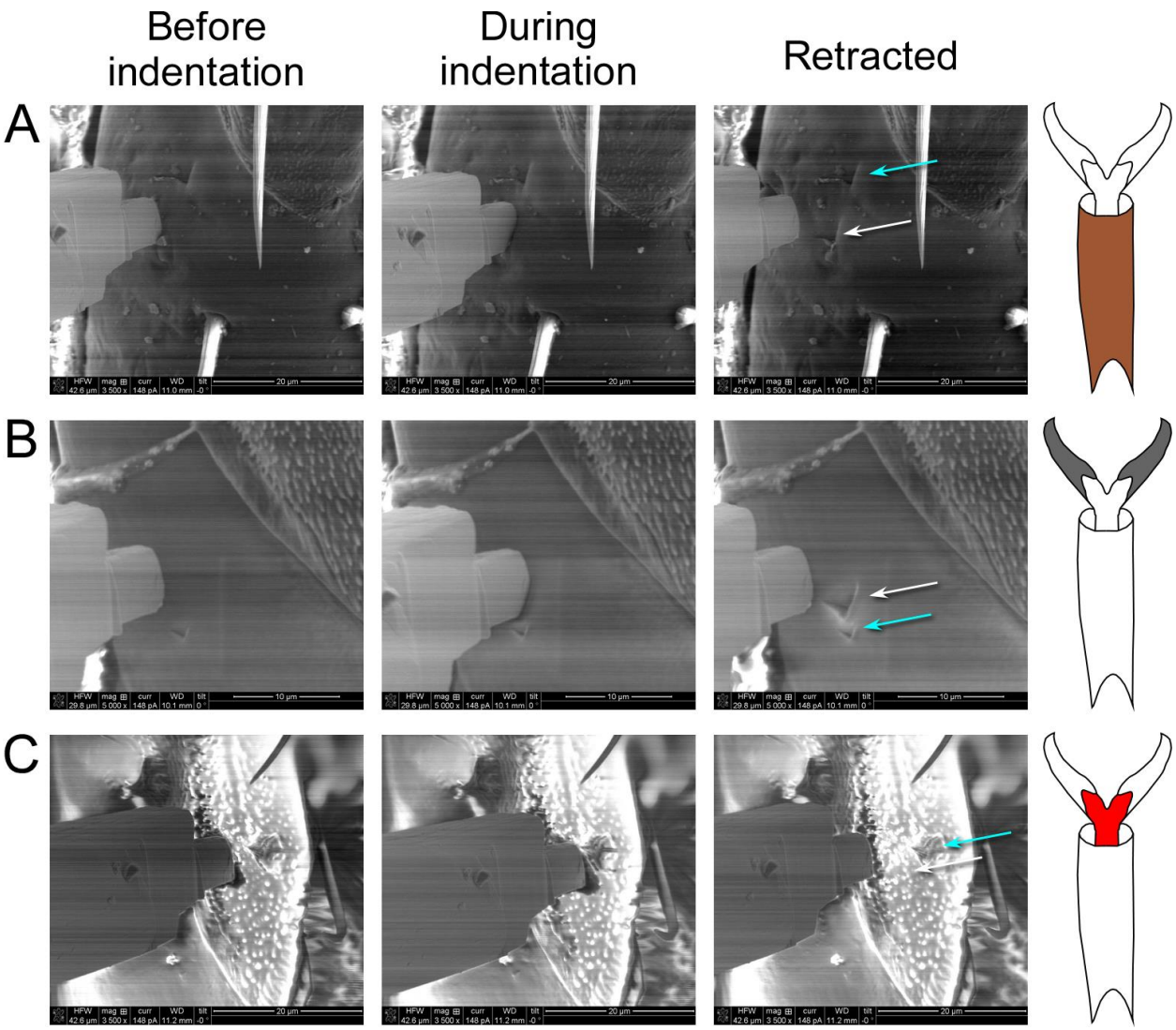

Figure 5. Scanning electron micrographs of nanomanipulator approaching cuticle, indenting into cuticle, and indent left after nanomanipulator is retracted. In each case a previous indent is visible (blue arrow) for comparison with the current indent (white arrow) A. Indent (3 microns) into tarsal subsegment 3; previous indent is also 3 microns. B. Indent (2 microns) into smooth part of claw; previous indent is 1 micron. C. Indent (2 microns) into membrane with microtrichia region of claw; previous indent is 8 microns.

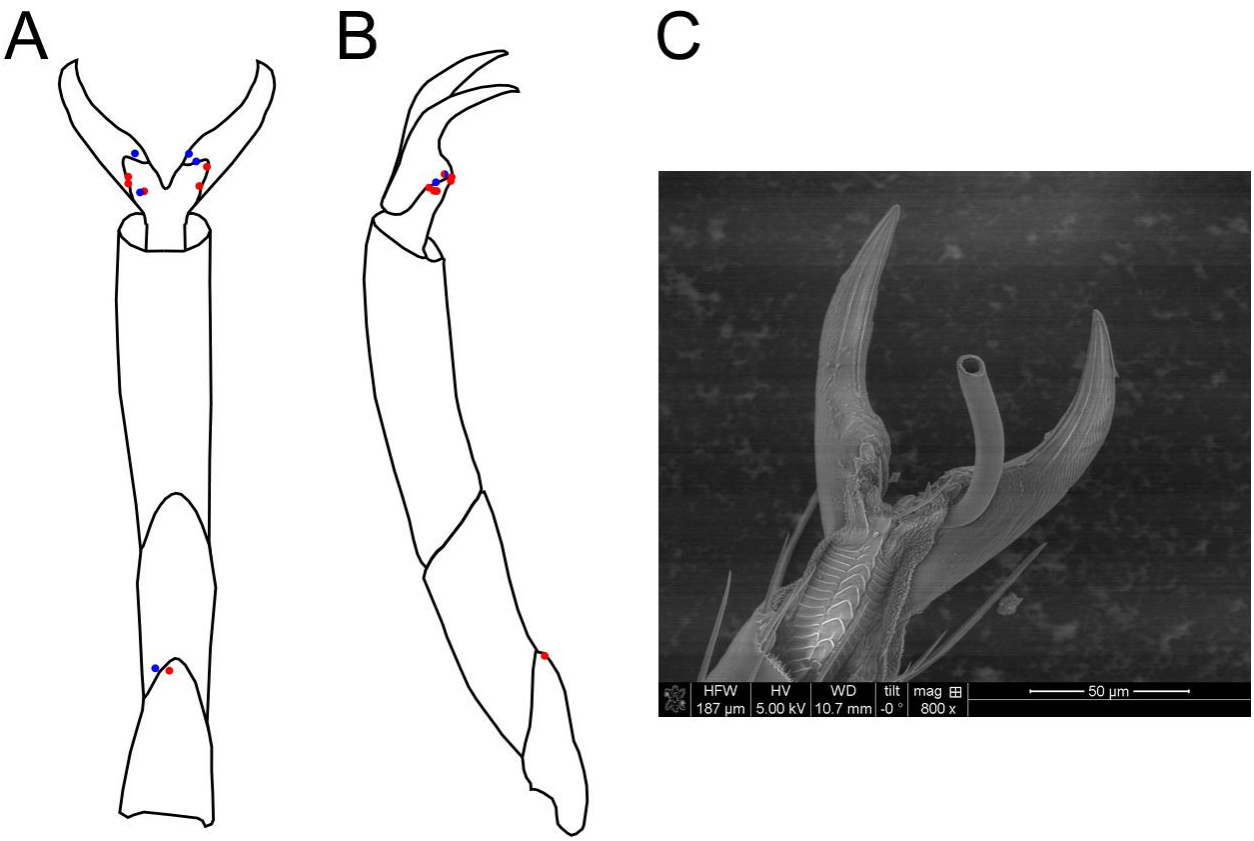

Figure 6. Pierced locations from multiple legs (from 10 bugs) are all shown on one leg to facilitate comparison. Each of the 19 red dots indicates the location where a trichome tip entered the cuticle (many are overlapping on the diagram), and each blue dot indicates an exit location. A. Ventral view of tarsus. B. Side view of tarsus. C. Scanning electron micrograph of ventral surface of pretarsal claw pierced by trichome (broken) in typical location.

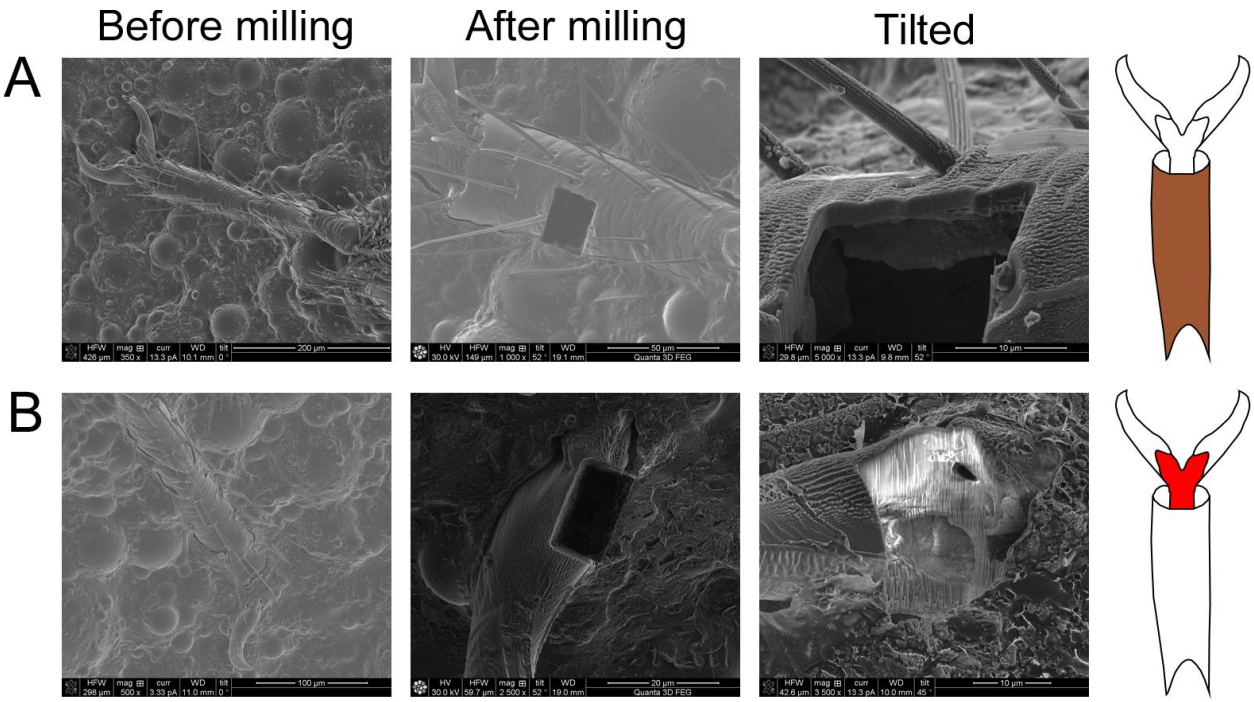

Figure 7. Scanning electron micrographs demonstrate how focused ion beam milling of tarsi was used to measure cuticle thickness. Left micrographs show tarsal structures before milling began. Middle micrographs show rectangular holes generated by milling. Right micrographs show structures tilted to view cut edges of cuticle. A. Milling on tarsal subsegment 3. B. Milling of pretarsal claw including smooth region and membrane with microtrichia.

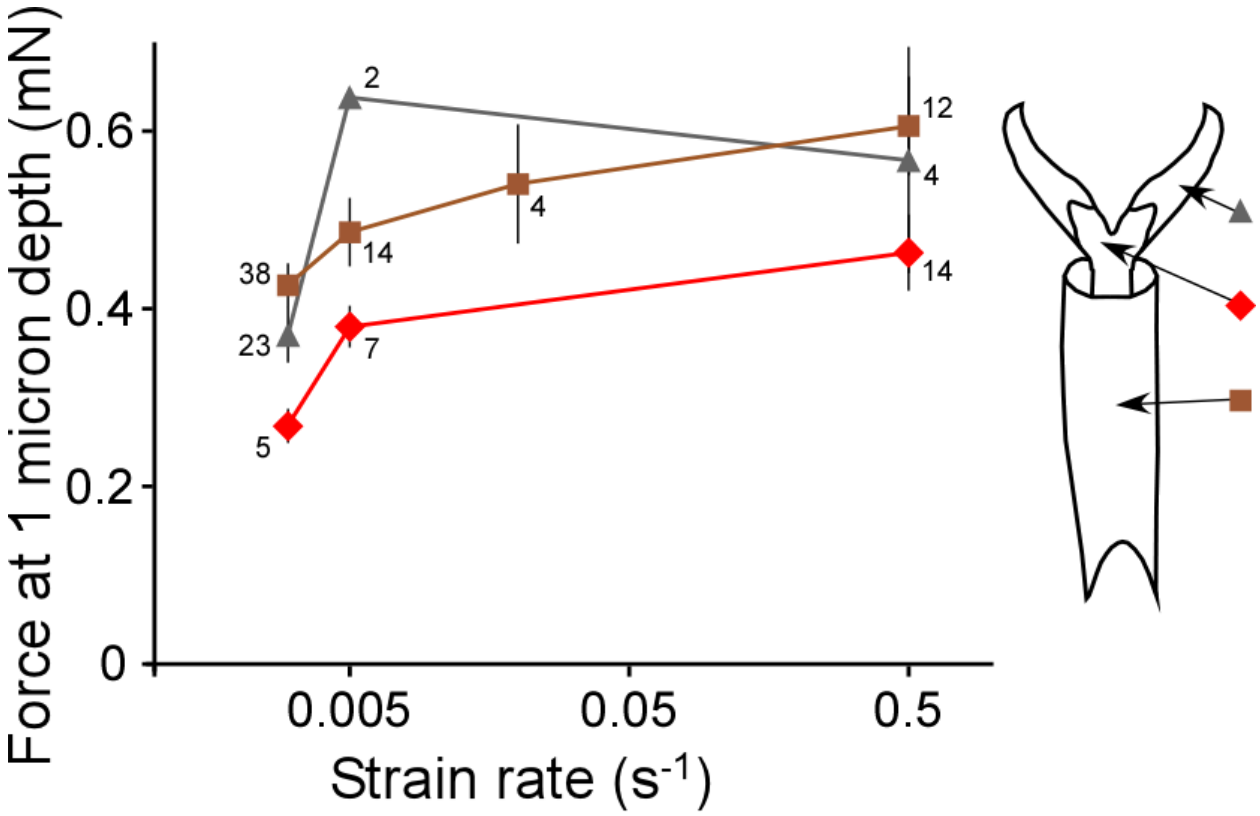

Figure 8. Force required to indent to a 1-micron depth as a function of strain rate and region of the tarsus being indented (mean ± 1 SE, sample size is indicated for each point; 123 indents illustrated overall). Regions: red diamonds indicate the membrane with microtrichia, grey triangles indicate the rest of the pretarsal claws, brown squares indicate the tarsal subsegments.

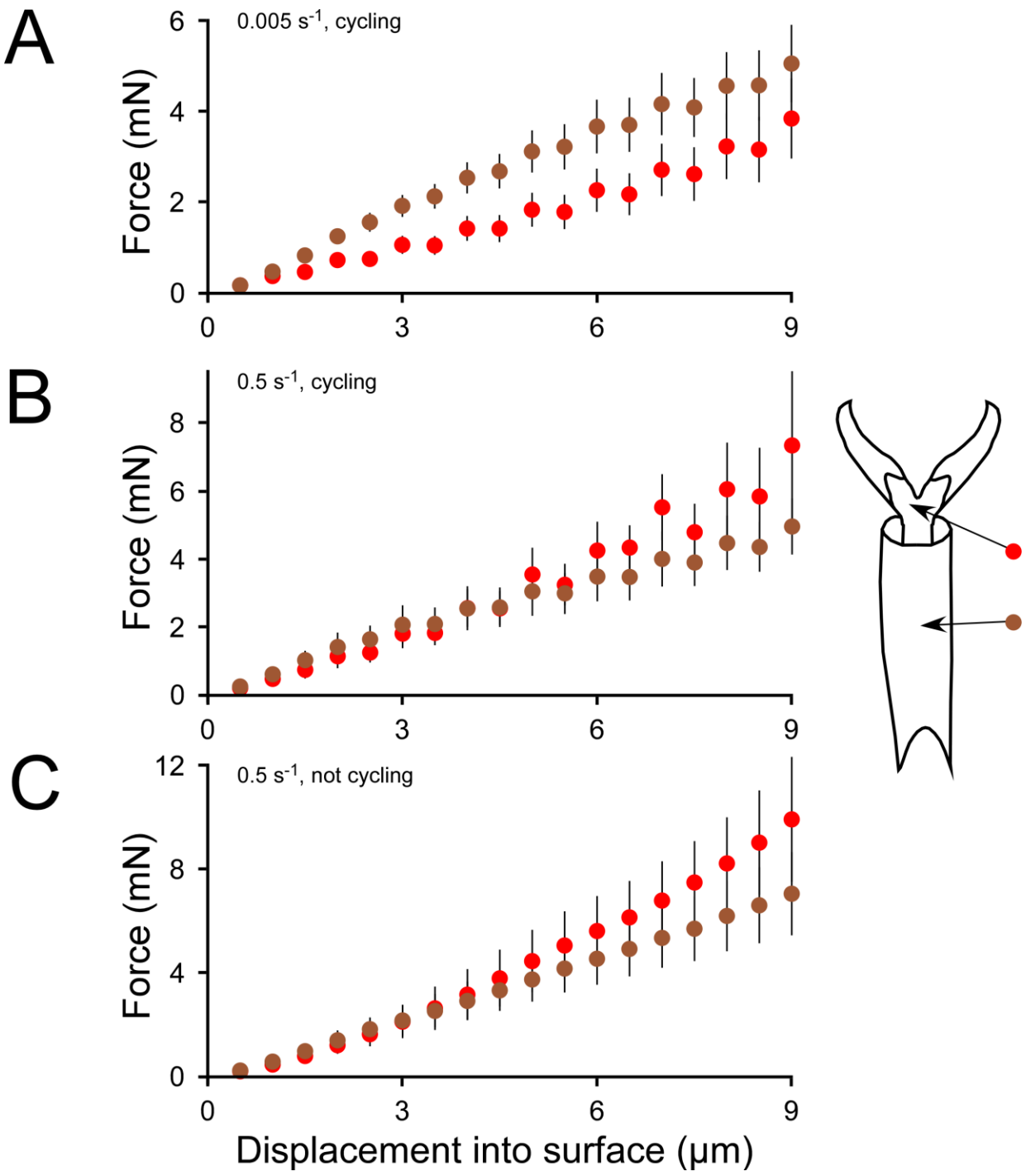

Figure 9. Force to indent to different depths as a function of region. A. Slow strain rate of 0.005 s^{-1}, cycling every micron (n = 8 for indents in tarsal subsegments, n = 7 for indents in membrane with microtrichia). B. Fast strain rate of 0.5 s^{-1}, cycling every micron (n = 6 for indents in tarsal

subsegments, n = 7 for indents in membrane with microtrichia). C. Fast strain rate of 0.5 s^{-1}, not cycling (n = 8 for indents in tarsal subsegments, n = 6 for indents in membrane with microtrichia). Each marker indicates the mean ± 2SE.

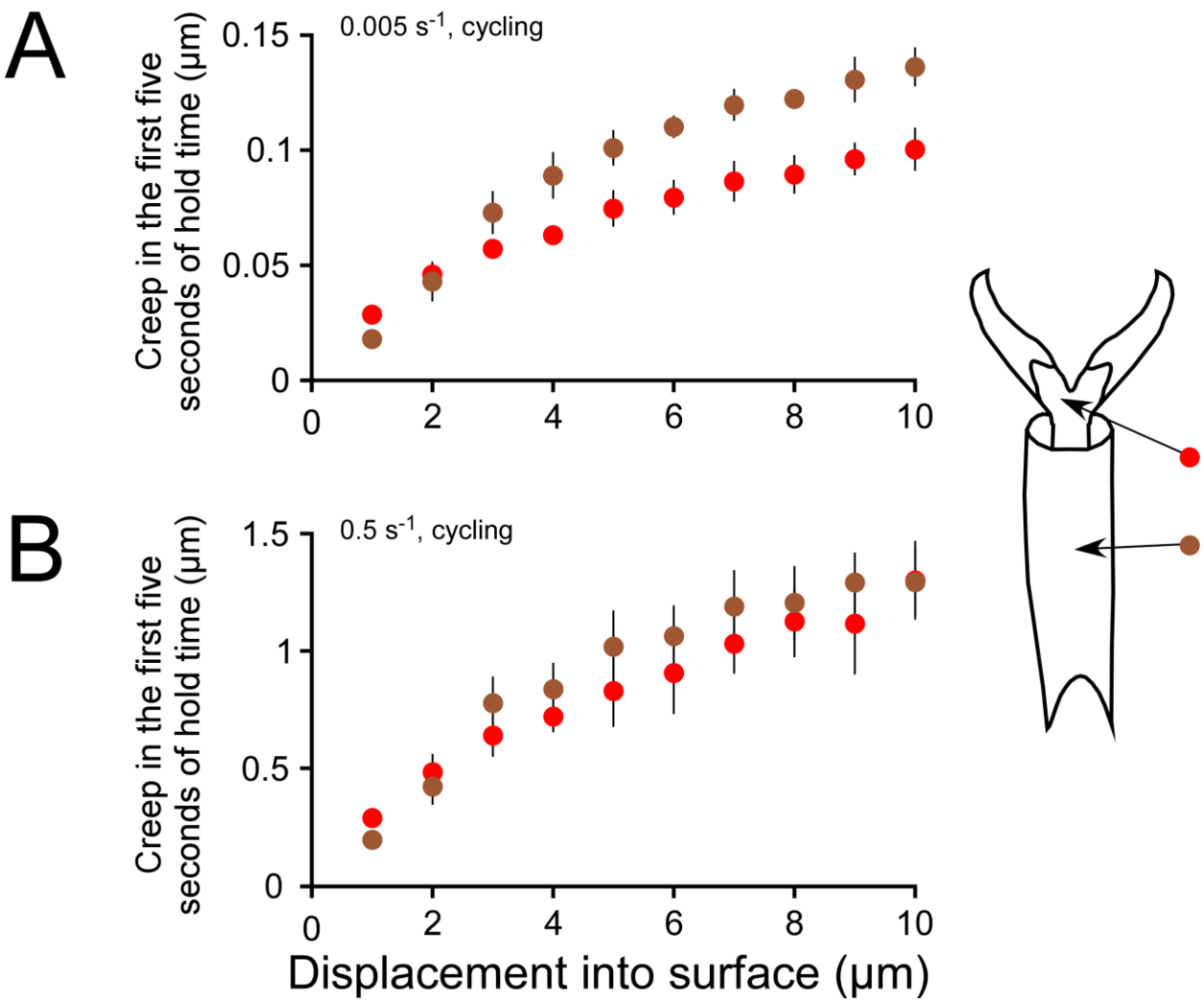

Figure 10. Creep for first 5 seconds of hold time as a function of strain rate and depth of indent. A. Slow strain rate of 0.005 s^{-1}, cycling every micron (*n* = 8 for indents in tarsal subsegments, *n* = 7 for indents in membrane with microtrichia). B. Fast strain rate of 0.5 s^{-1}, cycling every micron (*n* = 7 for indents in tarsal subsegments, *n* = 6 for indents in membrane with microtrichia). Each marker indicates the mean ± 2SE. Data for the smooth tarsal subsegments are not shown because the sample size is small (n = X); they overlap with the tarsal subsegment data.

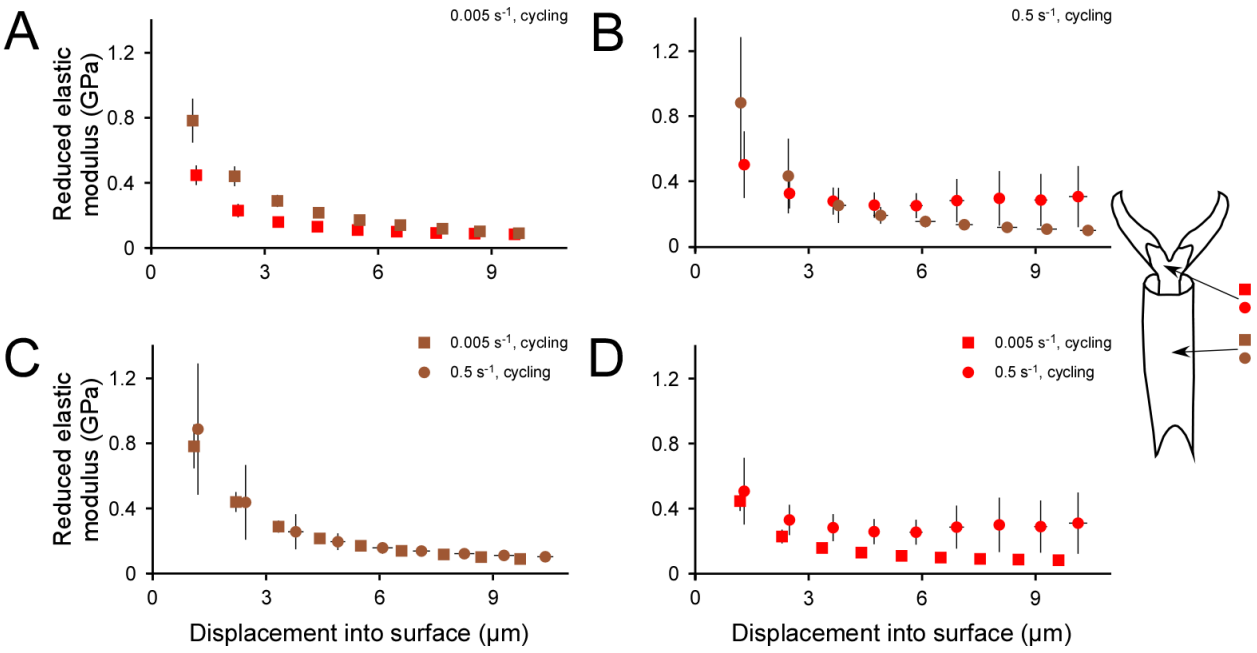

Figure 11. Reduced elastic modulus as a function of displacement during nanoindentation. A. Slow strain rate only, comparing the two regions. B. Fast strain rate only, comparing the two regions. C. Tarsal subsegment 3 only, comparing the two strain rates. D. Claw (membrane with microtrichia) only, comparing the two strain rates. Each marker indicates the mean ± 2SE for both y and x. Sample sizes: for slow strain rates, n = 8 for indents in tarsal subsegments, n = 7 for indents in membrane with microtrichia; for fast strain rates, n = 7 for indents in tarsal subsegments, n = 6 for indents in membrane with microtrichia.

REFERENCES

Barbakadze, N., Enders, S., Gorb, S. and Arzt, E. (2006). Local mechanical properties of the head articulation cuticle in the beetle *Pachnoda marginata* (Coleoptera, Scarabaeidae). *The Journal of Experimental Biology* **209**, 722-730.

Broomell, C. C., Zok, F. W. and Waite, J. H. (2008). Role of transition metals in sclerotization of biological tissue. *Acta Biomaterialia* **4**.

Cribb, B. W., Lin, C.-L., Rintoul, L., Hasenpusch, J. and Huang, H. (2010). Hardness in arthropod exoskeletons in the absence of transition metals. *Acta Biomaterialia* **6**, 3152-3156.

Doggett, S. L., Dwyer, D. E., Peñas, P. F. and Russell, R. C. (2012). Bed bugs: clinical relevance and control options. *Clinical Microbiology Reviews* **25**, 164-192.

Hansen, J. D., Johnson, J. A. and Winter, D. A. (2011). History and use of heat in pest control: a review. *International Journal of Pest Management* **57**, 267-289.

Huja, S. S., Hay, J. L., Rummel, A. M. and Beck, F. M. (2010). Quasi-static and harmonic indentation of osteonal bone. *Journal of Dental Biomechanics* **1**.

Johnson, B. (1953). The injurious effects of the hooked epidermal hairs of french beans (*Phaseolus-vulgaris* L) on *Aphis-craccivora* Koch. *Bulletin of Entomological Research* **44**, 779-788.

Kells, S. (2006a). Bed bugs: a systemic pest within society. *American Entomologist* **52**, 107-108.

Kells, S. (2006b). Nonchemical control of bed bugs. *American Entomologist* **52**, 109-110.

Kheireddin, B. A., Williams, T. C. and Akbulut, M. (2012). Tribological properties of femur–tibia articulation of lubber grasshopper. *Tribology International* **50**, 76-81.

Kinney, J. H., Marshall, S. J. and Marshall, G. W. (2003). The mechanical properties of human dentin: A critical review and re-evaluation of the dental literature. *Critical Reviews in Oral Biology and Medicine* **14**, 13-29.

Klein, C. A. (1992). Anisotropy of Young's modulus and Poisson's ratio in diamond. *Materials Research Bulletin* **27**, 1407-1414.

Klocke, D. and Schmitz, H. (2012). Material properties of photomechanical infrared receptors in pyrophilous *Melanophila* beetles and *Aradus* bugs. *Acta Biomaterialia* **8**, 3392–3399.

Koganemaru, R. and Miller, D. M. (2013). The bed bug problem: Past, present, and future control methods. *Pesticide Biochemistry and Physiology* **106**, 177-189.

Kohane, M., Daugela, A., Kutomi, H., Charlson, L., Wyrobek, A. and Wyrobek, J. (2003). Nanoscale *in vivo* evaluation of the stiffness of *Drosophila melanogaster* integument during development. *Journal of Biomedical Materials Research Part A* **66A**.

Muller, M., Olek, M., Giersig, M. and Schmitz, H. (2008). Micromechanical properties of consecutive layers in specialized insect cuticle: the gula of *Pachnoda marginata* (Coleoptera, Scarabaeidae) and the infrared sensilla of *Melanophila acuminata* (Coleoptera, Buprestidae). *Journal of Experimental Biology* **211**, 2576-2583.

Ngan, A. H. W., Wang, H. T., Tang, B. and Sze, K. Y. (2005). Correcting power-law viscoelastic effects in elastic modulus measurement using depth-sensing indentation. *International Journal of Solids and Structures* **42**, 1831-1846.

Oliver, W. C. and Pharr, G. M. (1992). An improved technique for determining hardness and elastic modulus using load and displacement sensing indentation experiments. *Journal of Materials Research* **7**, 1564-1583.

Potter, M. F. (2011). The history of bed bug management- with lessons from the past. *American Entomologist* **57**, 14-25.

Richardson, H. H. (1943). The action of bean leaves against the bed bug. *Journal of Economic Entomology* **36**, 543-544.

Sample, C. S., Xu, A. K., Swartz, S. M. and Gibson, L. J. (2015). Nanomechanical properties of wing membrane layers in the house cricket (*Acheta domesticus* Linnaeus). *Journal of Insect Physiology* **74**, 10-15.

SAS Institute, Inc. (2008). SAS/STAT 9.2 User's Guide. Cary, NC: SAS Institute Inc.

Snodgrass, R. E. (1935). Principles of Insect Morphology. New York: McGraw-Hill.

Szyndler, M. W., Haynes, K. F., Potter, M. F., Corn, R. M. and Loudon, C. (2013). Entrapment of bed bugs by leaf trichomes inspires microfabrication of biomimetic surfaces. *Journal of the Royal Society Interface* **10**.

Vincent, J. F. V. (1990). Structural Biomaterials. Princeton, NJ: Princeton University Press.

Voigt, D., Gorb, E. and Gorb, S. (2007). Plant surface-bug interactions: *Dicyphus errans* stalking along trichomes. *Arthropod-Plant Interactions* **1**, 221-243.

Voigt, D. and Gorb, S. (2010). Locomotion in a sticky terrain. *Arthropod-Plant Interactions*, 1-11.

Woodward, T. E., Evans, J. W. and Eastop, V. F. (1970). Hemiptera. In *The Insects of Australia*, pp. 387-1029. Melbourne, Australia: Melbourne University Press.

Xiao, K., Bai, K., Wang, W. and Song, F. (2007). Experimental study on the microstructure and nanomechanical properties of the wing membrane of dragonfly. *Acta Mechanica Sinica* **23**, 281-285.